Developing Wave Packets in the North Pacific Storm Track

GREGORY J. HAKIM

Department of Atmospheric Sciences, University of Washington, Seattle, Washington

(Manuscript received 3 September 2002, in final form 9 May 2003)

ABSTRACT

Developing wave packets in the western North Pacific storm track are diagnosed observationally. An abrupt upstream edge to baroclinic wave activity over the western North Pacific facilitates comparisons between the observational results and previous theoretical predictions on the spatiotemporal evolution of an impulse disturbance. Results show that surface cyclogenesis events are preceded by a sharply peaked wave packet that originates poleward of the Himalaya Plateau and develops rapidly across the North Pacific to North America.

Composite wave-packet structure is broadly consistent with linear theory for idealized models such as Eady's. The longitude–height structure of the mature packet reveals deep growing waves with horizontal wavelengths of approximately 4000 km near the packet peak. Downstream from the peak, amplitude decays exponentially, and wavelength decreases approximately linearly to about 2500–3000 km at the leading edge. Meridional potential vorticity gradients are concentrated near the tropopause. In contrast to linear theory, the packets show an abrupt upstream edge and no evidence of upstream development. As the packet travels through the along-stream variations of the Pacific jet stream, the packet-peak and leading-edge group velocity vary. These accelerations change the packet length and suggest that the Pacific jet may act to focus the packets.

A sample of North Atlantic storm track events reveals similar results and suggests that the Atlantic storm track is often seeded by wave packets that originate over the western North Pacific Ocean. In contrast, Atlantic packets refract equatorward and become trapped on the subtropical jet to the south of Himalaya Plateau, suggesting perhaps less potential for seeding disturbances in the Pacific storm track.

1. Introduction

Downstream development is often envisioned as the successive appearance of troughs and ridges downstream from an existing trough or ridge. This behavior is usually associated with the formation of wave packets and the dispersive character of baroclinic waves that populate the storm tracks. There has been intense interest in downstream development and wave packets in the past decade, and the climatology of these features is well documented (e.g., Chang and Yu 1999; Chang 1999). Relatively less attention has been devoted to observations of the structure of developing wave packets that arise from impulsive disturbances, such as localized cyclogenesis. In this paper I concentrate on comparing observed impulse evolution with theoretical predictions and on how downstream development in the North Pacific storm track spreads toward North America and locations farther east, including the extent to which the Northern Hemisphere storm tracks seed one another.

Although the roots of downstream-development research trace back to earlier research by Namias and Clapp (1944) and Cressman (1948), these studies viewed downstream development as the dispersion of neutral-plane Rossby waves; as we discuss below, this view is incomplete when unstable waves exist, such as in the storm tracks. Modern work on downstream development follows from Simmons and Hoskins's (1979) analysis of spreading disturbances on an idealized unstable jet stream. Observational support for the importance of this process was subsequently discovered through case studies (Orlanski and Katzfey 1991; Chang 2000) and statistical analysis of storm tracks (Chang 1993, 1999; Chang and Yu 1999). These studies show that a significant source of energy for developing cyclones is due to downstream radiation from existing upstream disturbances. Furthermore, a new view on the life cycle of cyclones has emerged, in which the primary decay mechanism is not a barotropic Reynolds stress on the background flow, but rather the downstream radiation of energy (Chang and Orlanski 1993; Orlanski and Gross 2000).

Several theoretical predictions that have not been considered previously are tested here observationally. In particular, we are interested in the properties of the packet between the peak and the leading edge. Linear theory predicts a decrease in horizontal wavelength and an increase in group velocity toward the leading edge; the

Corresponding author address: Dr. Gregory J. Hakim, Dept. of Atmospheric Sciences, University of Washington, Box 351640, Seattle, WA 98195-1640.
E-mail: hakim@atmos.washington.edu

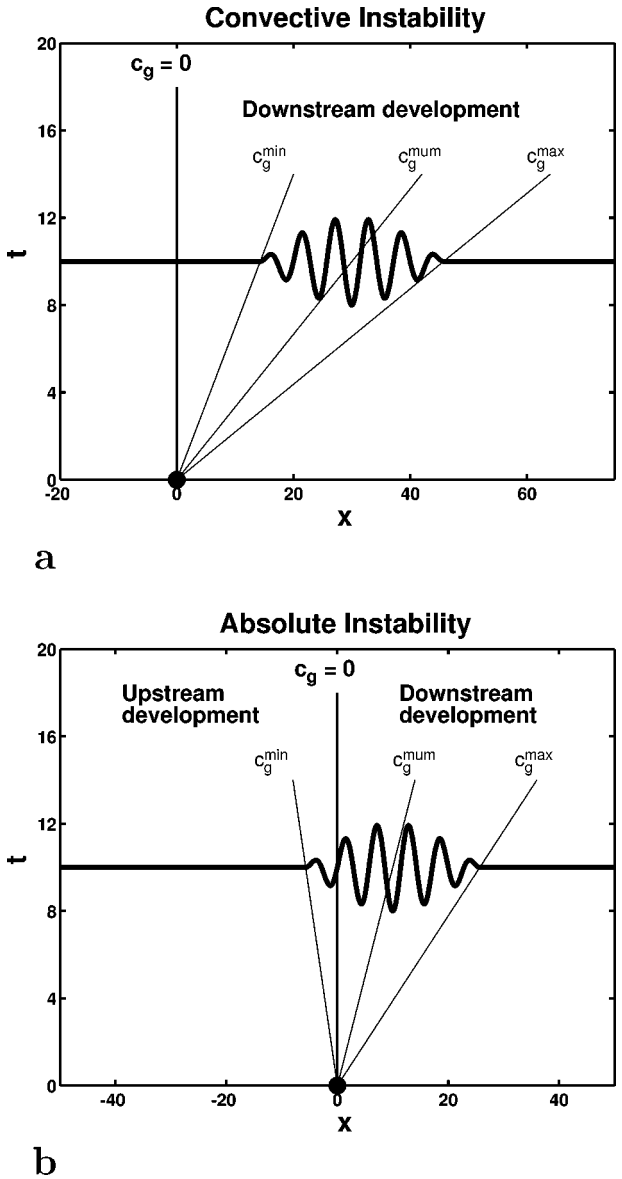

FIG. 1. Schematic depictions of the spatiotemporal evolution of an impulse disturbance for flows that are (a) convectively unstable and (b) absolutely unstable. The heavy black line denotes the wave packet, and the thin lines represent the three critical rays on the x–t plane: the leading ray (C_g^{max}), the peak ray (C_g^{mum}), and the trailing ray (C_g^{min}). Absolutely unstable flows are characterized by (C_g^{max}) and (C_g^{min}) having opposite sign and, therefore, supporting both upstream and downstream development.

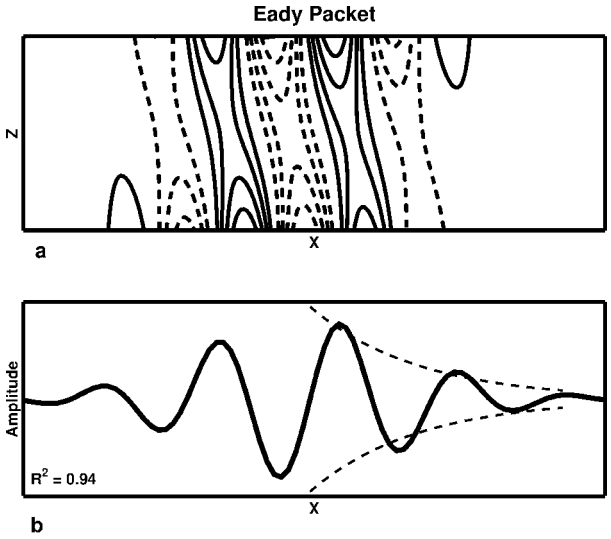

FIG. 2. Wave-packet development in the linear Eady model. (a) Zonal–height (x–z cross section) of perturbation pressure (arbitrary contour interval) and (b) zonal amplitude profile on the top boundary. The dashed line in (b) represents an exponential fit to the leading edge of the packet using the method applied to observed cases. The depicted domain is 20 000 km long and 10 km deep. Note that there is no Ekman damping, which would reduce disturbance amplitude at the surface relative to the tropopause.

speed of the leading edge is predicted to be bounded above by the jet-level winds. The observational analysis in section 4 is consistent in many respects with these predictions, although packet properties vary in time as the packets propagate through along-stream variations in the Pacific jet stream. When filtered to a common ray path, a sample subset drawn from all events at 45°N is shown to persist for at least 10 days; however, subtropical absorption and strong along-jet variability appear to persistently attenuate mature wave packets. Finally, the results also suggest that the Pacific jet may ''seed'' wave activity in the Atlantic jet, but the reverse is less likely; wave packets spawned in the Atlantic tend to refract into the subtropical jet over Asia, whereas Pacific jet precursor disturbances originate over higher latitudes.

Theoretical predictions are summarized in section 2, and the methods employed to test these predictions on observed data are summarized in section 3. Results are presented in section 4, followed by conclusions in section 5.

2. Theoretical background

Dispersion of energy is a celebrated property of fluids for which linear wave frequency, σ, varies with wavenumber, k. More precisely, because energy is transported by the group velocity, $c_g = \partial\sigma/\partial k$, dispersion requires the group velocity to be a function of wavenumber. Perhaps the most familiar example of this phenomenon is the dispersion of nondivergent-barotropic-plane Rossby waves away from an initially localized disturbance (e.g., Pedlosky 1987, section 3.24). When plotted on the space–time (x–t) plane, the essential properties of the spreading disturbance may be summarized at later times by three straight lines, or rays. The ''peak'' ray defines the location of the packet peak, which moves with the group velocity of the wave having the largest amplitude. The ''leading'' and ''trailing'' rays define the leading and trailing edges

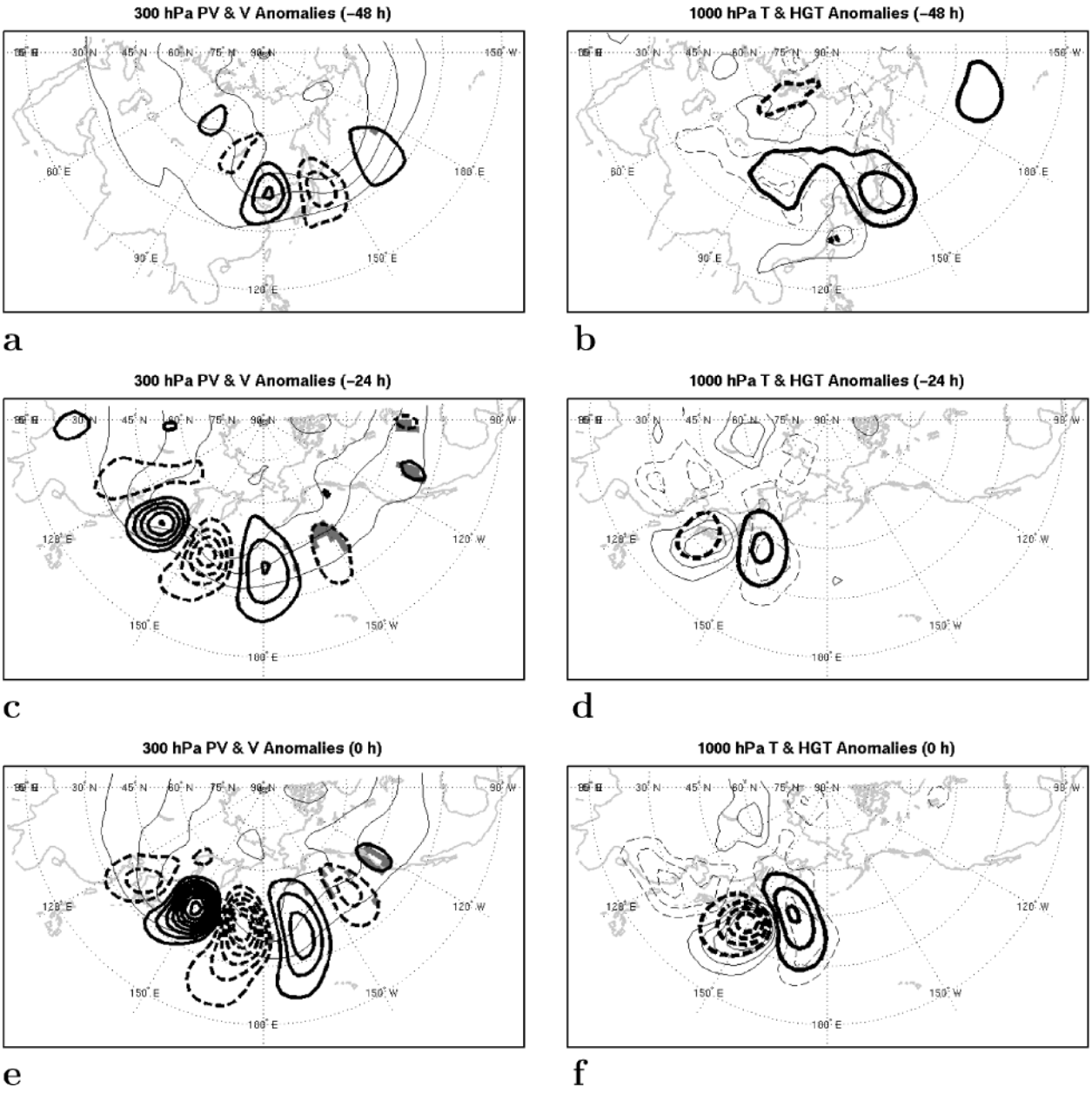

FIG. 3. Ensemble-mean time evolution of the Pacific wave packets at (a), (c), (e), (g), (i), and (k) 300 hPa and (b), (d), (f), (h), (j), (l) 1000 hPa. At 300 hPa, the anomaly meridional wind is given by heavy lines every 2 m s^{-1}, except 1 m s^{-1} in (k); the Ertel PV is given by thin solid lines every 1 PVU starting from 1 PVU [1 PVU = 10^{-6} m^2 K (kg s)$^{-1}$]. At 1000 hPa, the anomaly geopotential height is given by heavy lines every 20 m, except every 10 m in (b) and (j) and every 5 m in (l); the anomaly temperature field is given by thin lines every 0.5°C from −2° to 2°C. The zero contour is suppressed in all fields, negative values are denoted by dashed lines, and shaded regions depict locations at 300 hPa that fail a Student's *t*-test for statistical significance at the 99% confidence level. Time increases downward in the figure by 24 h per row, and the central longitude in the figure shifts eastward with time.

of the disturbance, which move with the maximum and minimum group velocity, respectively.

This simple picture is modified in the presence of growing and decaying waves, as in the case of extratropical storm tracks. The analysis of this problem is more complicated than the neutral wave case, so we limit the discussion to those aspects that we wish to test observationally [for further details, the interested reader may consult Huerre and Monkewitz (1990) and Pierrehumbert and Swanson (1995)]. The time evolution of an initially localized disturbance in unstable flow differs from the neutral case in that at later times the packet peak travels with the group velocity of the unstable wave having the largest growth rate. The leading and trailing rays are defined by the fastest and slowest speeds for which a moving observer notices wave growth. Since these pack-

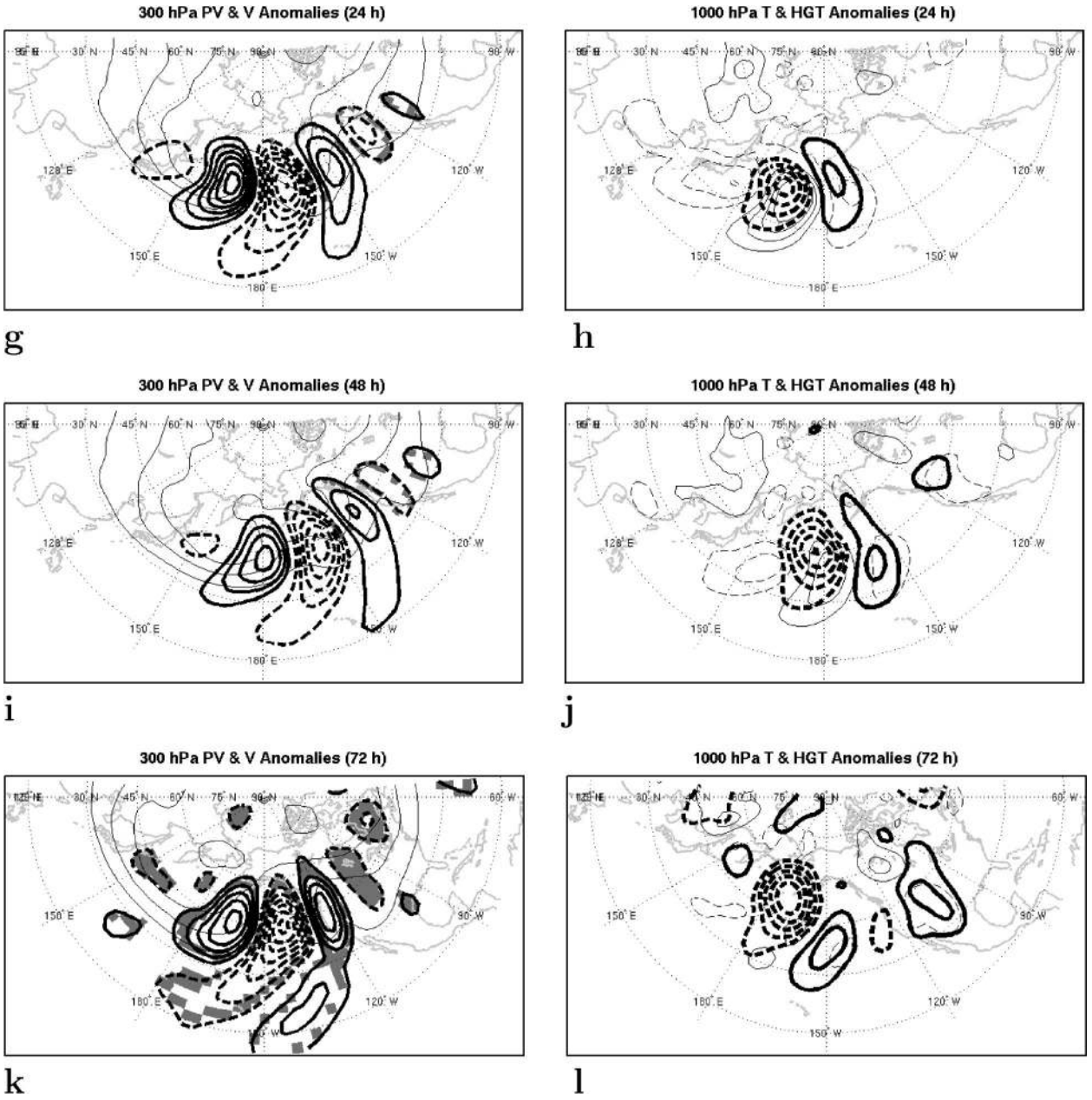

FIG. 3. (*Continued*)

ets spread in space as well as time, an imaginary wavenumber, which is analogous to an imaginary frequency, describes the exponential decay of packet amplitude away from the packet peak (e.g., Briggs 1964).

Downstream development shall be defined as the spreading of wave activity toward the ''east'' ($x > 0$) and upstream development as spreading toward the ''west'' ($x < 0$).[1] When only downstream development occurs, the flow is called ''convectively'' unstable because although the packet is spreading and growing it eventually passes a stationary observer; at a fixed point, there is no exponential growth in the long-time limit (Fig. 1a). Conversely, when both upstream and downstream development occur, the flow is called ''absolutely'' unstable because the disturbance eventually affects every location; a stationary observer sees exponential growth in the long time limit (Fig. 1b). It should be noted that these definitions are strictly valid only for nonperiodic domains; however, the concepts are still useful for periodic domains during short time intervals.

[1] This definition is motivated by the important distinction between absolute and convective instability; however, we note that it differs from common meteorological usage that defines upstream development relative to the incipient cyclone (Simmons and Hoskins 1979).

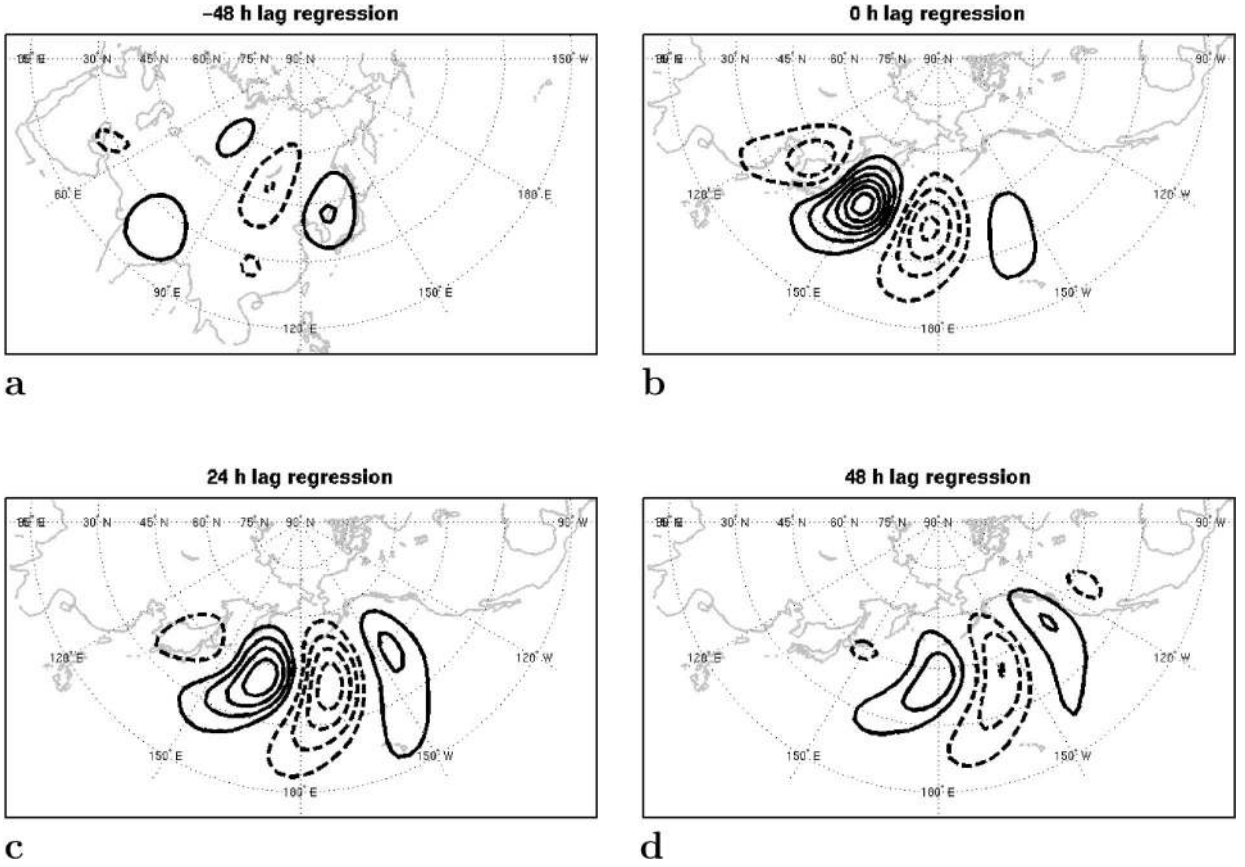

FIG. 4. Ensemble-mean regression maps of 300-hPa meridional wind for a reference time series at 40°N, 152.5°E for lags of (a) −48, (b) 0, (c) 24, and (d) 48 h. The contour interval is 2 m s^{-1}, and the regression integral was performed over a ±10 day window surrounding $t = 0$.

It will be shown in section 4a that near wave packets the troposphere has a nearly homogeneous distribution of potential vorticity (PV), with large meridional gradients concentrated near the tropopause. This observation suggests that the relevant theories to test are those based on homogeneous-PV models, the simplest of which is Eady's (1949) model. An example of localized impulse development in the Eady model is illustrated in Fig. 2. A linear analysis of this problem shows that packet properties near the peak (e.g., wavelength and group speed) are indeed defined by the most unstable mode (Simmons and Hoskins 1979; Farrell 1983). Moving toward the leading edge of the packet, one notices a decrease in the local wavelength and growth rate and an increase in the local phase and group speeds; in the limit as one approaches the leading edge of the packet, local wavenumber tends to infinity, local growth rate tends to zero, and local phase and group speed tend to the background-flow speed (Farrell 1983). Upstream development, and therefore absolute instability, requires easterly winds at the surface, which are unlikely in the storm tracks. Another impediment to upstream development, which spreads first at the surface, is frictional damping.

Similar results are obtained for more general idealizations of a storm track (Pierrehumbert 1984; Whitaker and Barcilon 1992; Orlanski and Chang 1993; Lee and Held 1993; Swanson and Pierrehumbert 1994). Essential nonlinear modifications include little variation in wavelength and a strong increase in the local phase speed toward the leading edge of the packet. Furthermore, the mature packet peak tends to move faster than in linear theory, approaching the speed of the leading edge (Swanson and Pierrehumbert 1994).

The analysis of observations represents an attempt to assess the theoretical predictions described above. In particular, a large sample of wave packets is examined to diagnose the three primary rays, the vertical structure of the packet, the zonal amplitude profile, and the variation of wavelength within the packet. The method of this analysis is described in the following section.

3. Method

The western North Pacific is selected for study since cyclogenesis events occur frequently in this region and an upstream edge to cyclogenesis is sharply defined because of the extensive upstream Eurasian landmass. This

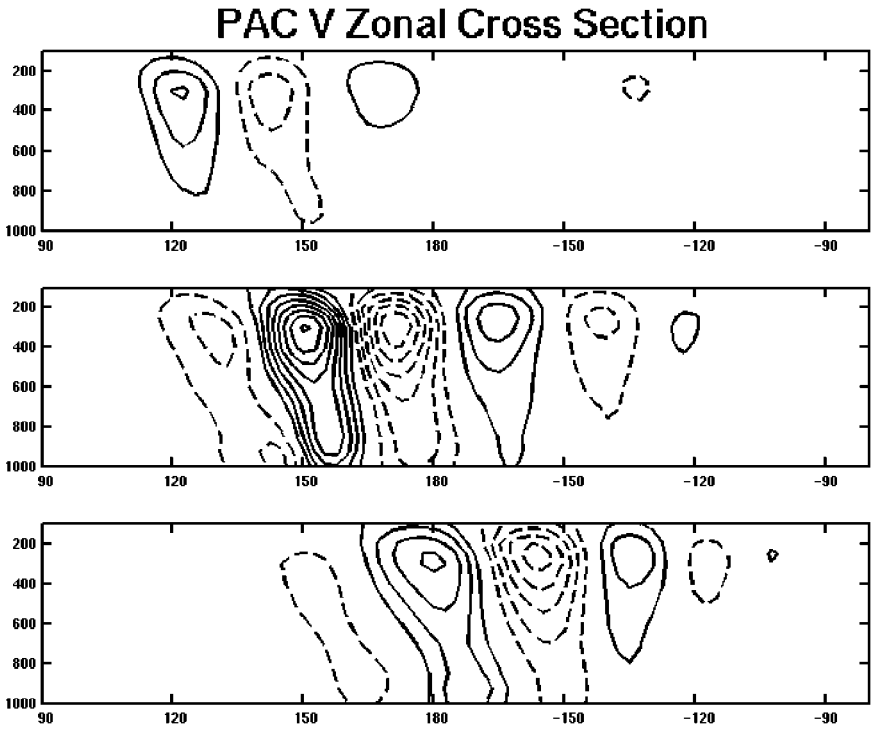

FIG. 5. Ensemble-mean longitude (°E)–pressure (hPa) cross sections of anomaly meridional wind for the Pacific wave-packet sample. Contours are drawn every 2 m s^{-1}, with negative values dashed. Cross sections are shown for (top) $t = -48$ h, (middle) $t = 0$ h, and (bottom) $t = 48$ h.

effective localization approximates the idealizations made in the theoretical studies described in section 2.

a. Event selection

The data used in this study is the National Centers for Environmental Prediction–National Center for Atmospheric Research (NCEP–NCAR) reanalysis dataset on mandatory constant pressure surfaces and a 2.5° × 2.5° latitude–longitude grid every 6 h. Cyclones are defined as local maxima in 1000-hPa geostrophic relative vorticity, ζ_g.[2] Only significant cyclones, those having $\zeta_g > 10^{-4}$ s^{-1}, are retained; the results are not sensitive to the exact threshold value. The period of study is November–March 1949–99, with anomaly fields defined relative to monthly means over this 51-yr period. Statistically significant anomalies are defined in terms of a two-side Student's t test with a threshold of 99%.

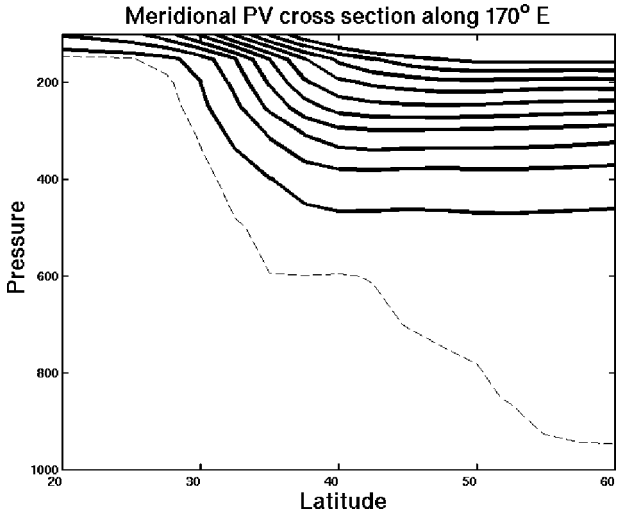

FIG. 6. Latitude (°N)–pressure (hPa) cross section of ensemble-mean Ertel PV for the Pacific wave-packet sample. Contours are drawn every 1 PVU from 1 to 10 PVU; the thin dashed line shows 0.5 PVU. The cross section is taken along 170°E at $t = 0$ h.

To enforce localization, cyclones that are located within 25° latitude and longitude of another cyclone at the same time are removed. Moreover, to insure that events are not sampled more than once, cyclones that are within 15° latitude and longitude of a previously identified cyclone during the previous 24 h are removed. We will refer to the time at which the cyclone is identified as "$t = 0$," which is approximately when the cyclone is reaching the mature stage.

A sample of Pacific (PAC) wave packets is defined by cyclones occurring over 35°–40°N, 145°–155°E, which represents a local maximum in regional cyclogenesis. Later in this paper the PAC results are compared to Atlantic (ATL) wave packets, which are defined by cyclones occurring over 37.5°–42.5°N, 65°–75°W,

[2] Geostrophic relative vorticity, ζ_g, is chosen because it has less small-scale noise than the actual relative vorticity.

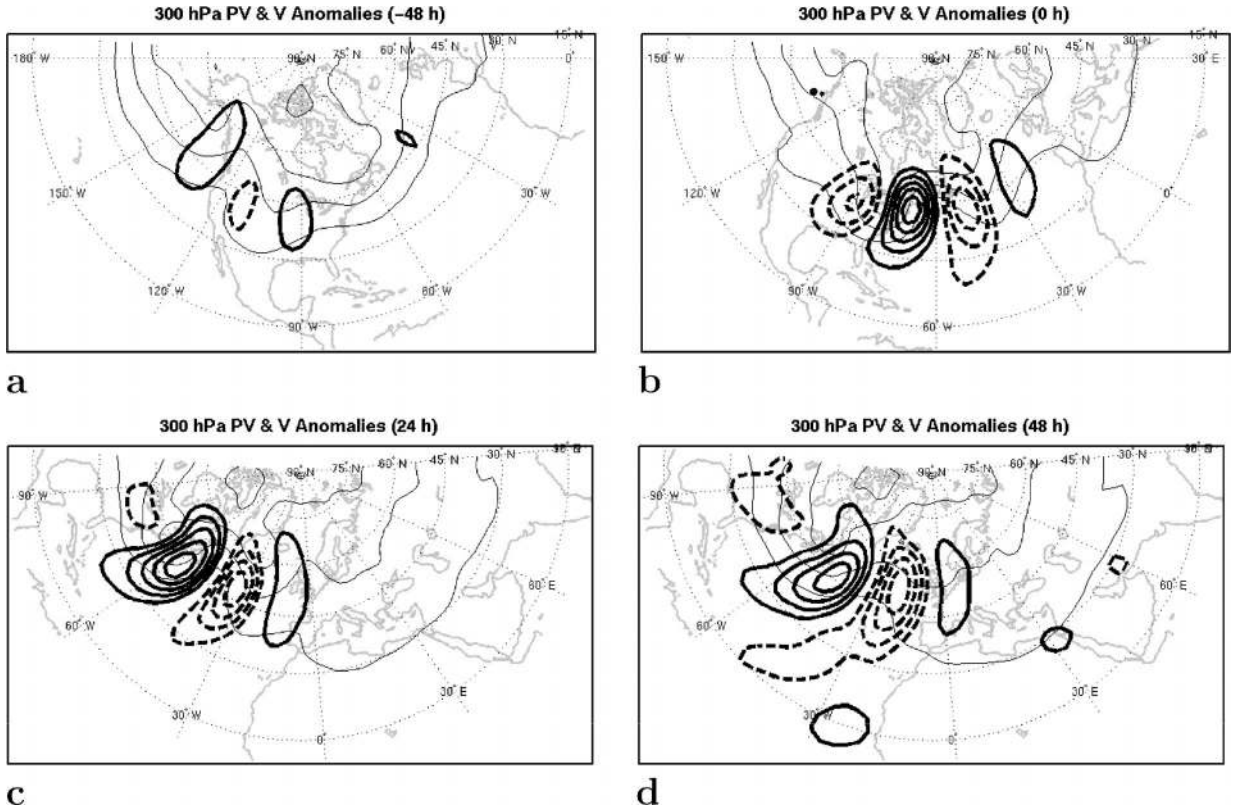

FIG. 7. Ensemble-mean time evolution of the Atlantic wave packets at 300 hPa for (a) $t = -48$ h, (b) $t = 0$ h, (c) $t = 24$ h, and (d) $t = 48$ h. Anomaly meridional wind is given by heavy lines every 3 m s^{-1} in (a) and (c), every 4 m s^{-1} in (b), and every 2 m s^{-1} in (d). Negative values are dashed and the zero contour is suppressed. Ertel PV is given by thin solid lines every 1 PVU starting from 1 PVU.

and all Northern Hemisphere (NH) wave packets, which are defined by cyclones occurring over 35°–40°N. There are a total of 382 PAC cases, 358 ATL cases, and 3338 NH cases.

b. Wave-packet analysis

The primary analysis technique is ensemble averaging for a range of time lags. For the PAC and ATL wave packets straightforward averaging is employed, whereas for the NH wave packets the events are shifted to a common longitude. Useful attributes of this method include its simplicity and the fact that it does not integrate away time and amplitude information, as occurs for time series regression and correlation analyses; that is, the signal of interest is not diluted with extraneous information. A disadvantage of the method is that the signal captured by the ensemble mean degrades for nonzero time lags because of the different trajectories and velocities for both individual eddies and the entire packets. In an attempt to reduce this effect, the sample populations are later limited to those following a common ray path (details are provided in section 4d).

Wave packets are analyzed to determine the three primary rays, the vertical structure of the packet, the zonal amplitude profile, and the variation of wavelength within the packet. At a particular time, the packet is identified in the 300-hPa meridional wind field over a 250° longitude window surrounding the maximum gridpoint value. The packet peak is defined by the maximum value of an interpolated polynomial that is fit to six gridpoint extrema surrounding the maximum value. Similarly, local extrema and zero crossings are defined by an interpolated polynomial that is fit to data near the packet. These data are then used to fit a curve defining the packet downstream from the packet peak using linear regression to an exponential profile; this fit worked well in all cases, including the idealized simulation shown in Fig. 2. The leading edge is defined as 2.5 *e*-folding distances from the packet peak, which corresponds to a location with ≈8% of the peak amplitude. Although this choice is arbitrary, it seems to match the location where the packet blends into the ambient noise of the background state. Interpolated extrema and zero-crossing data are used to calculate wavelength as a function of position within the packet.

4. Results

a. Pacific cyclones

Composites for the PAC cyclogenesis events show that 48 h prior to the time the 1000-hPa cyclone reaches

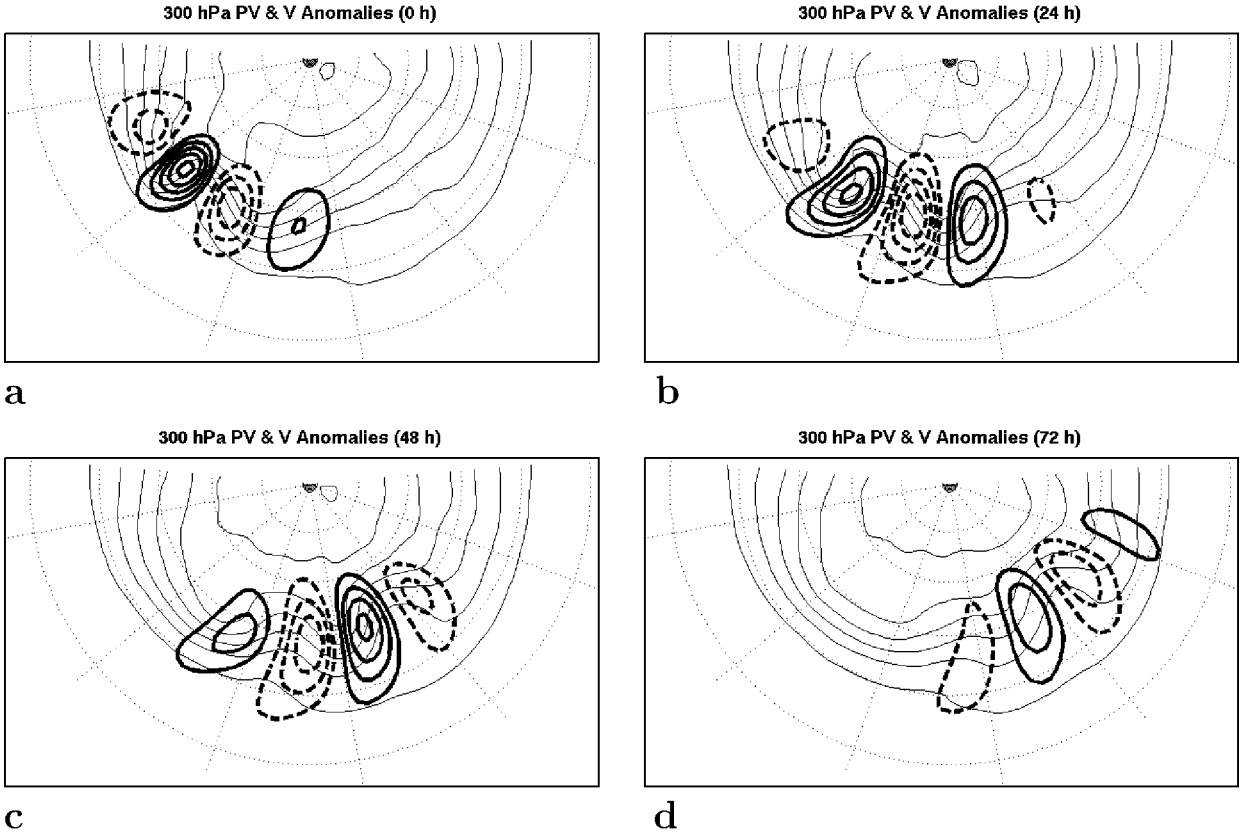

FIG. 8. Ensemble-mean time evolution of the Northern Hemisphere wave packets at 300 hPa for (a) $t = 0$ h, (b) $t = 24$ h, (c) $t = 48$ h, and (d) $t = 72$ h. Anomaly meridional wind is given by heavy lines every 4 m s^{-1}. Negative values are dashed and the zero contour is suppressed. Ertel PV is given by thin solid lines every 1 PVU starting from 1 PVU. Relative latitude and longitude lines are shown dotted every 15° and 30°, respectively.

the threshold criteria (i.e., $t = 0$), a sharply peaked wave packet is located near eastern China (Fig. 3a). At 1000 hPa, the dominant signal is an anticyclone over Japan, with northerly geostrophic flow advecting anomalously cold air over the coastal ocean (Fig. 3b). This precursor disturbance may contribute to preconditioning the lower troposphere for the subsequent primary cyclogenesis (Gyakum et al. 1992). A nascent cyclone and anomalously warm air are found over southeast China. The 1000-hPa cyclone–anticyclone pair continue to amplify and move east over the next 48 h.

At 300 hPa, the wave packet expands and amplifies across the Pacific Ocean over the next 48 h (Figs. 3c,e). Undulations in the Ertel potential vorticity field near and east of the date line at $t = 0$ show that the PV anomalies are partially in-phase with the meridional wind anomalies, indicating growth of the PV anomalies downstream from the packet peak. At $t + 24$ h, the composite 1000-hPa cyclone exhibits a cold front in both the anomalous geopotential height and temperature fields (Fig. 3h). Over the next 48 h, the cyclone moves northeastward and weakens. There is little in the way of new 1000-hPa disturbance development over the eastern Pacific Ocean, which could be due to phase scrambling at large time lags. Nevertheless, there is a statistically significant signal for weak anomalously high geopotential height over the northwestern United States at $t + 72$ h, with anomalously warm air in a region of downslope westerly geostrophic winds (Fig. 3l). Aloft, the wave packet continues to move across the Pacific Ocean, following a meridional PV gradient, so that by $t + 72$ h the peak is located in the Gulf of Alaska (Fig. 3k). The southern edge of the packet exhibits refraction deep into subtropical latitudes, reaching the equator in some locations (not shown).

For purposes of comparison, Fig. 4 shows the ensemble-mean one-point regression maps for 300-hPa meridional wind. Following Lim and Wallace (1991), all gridpoint time series are regressed against a normalized reference time series near the PAC base point (40°N, 152.5°E); the calculation is performed over a ± 10 day window surrounding $t = 0$. Although the results are qualitatively in agreement with the ensemble-mean results of Fig. 3, there are important differences. The packet amplitude is considerably weaker and the horizontal scale of the waves is longer in the regression results. Moreover, the regression results show the precursor disturbance as two separate wave trains that merge over

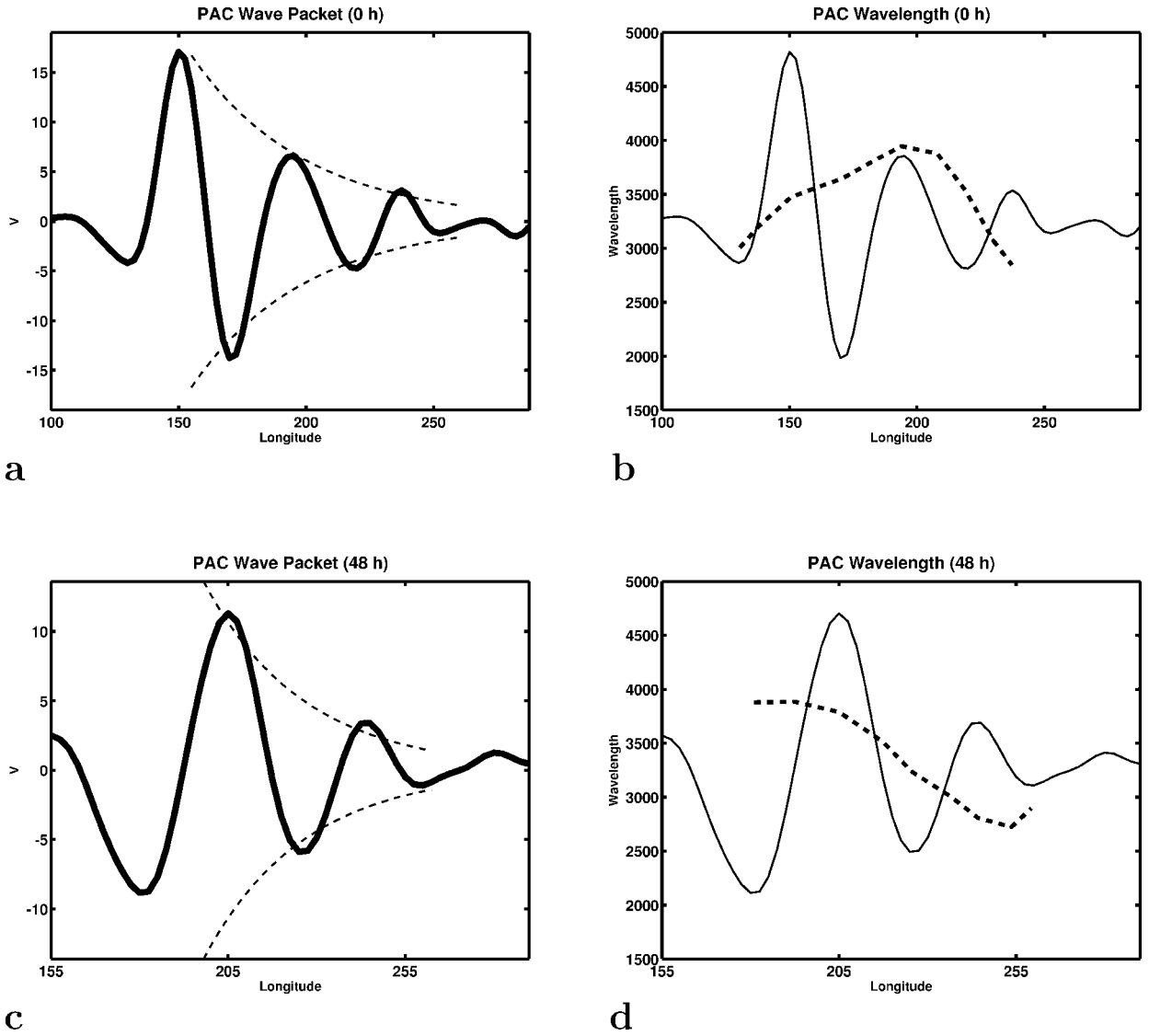

FIG. 9. Pacific wave-packet analysis at (a), (b) $t = 0$ h and (c), (d) $t = 48$ h. Solid lines depict the anomaly meridional wind (m s^{-1}) as a function of longitude at 42.5°N. Dashed lines in (a) and (c) show the linear fit to an exponential profile from the packet peak to 2.5 *e*-folding distances downstream from the peak. Dashed lines in (b) and (d) show the local wavelength (km) within the packet as a function of longitude. Details on the calculation are given in section 3b.

the western Pacific. These results reflect the fact that the regression calculation is an integral over time and therefore dilutes the relatively delicate signal associated with an initial-value problem. Indeed, the regression results are sensitive to the length of time integration, with longer time periods increasingly weighted by climatological information.

A zonal cross section through the developing packet exhibits patterns that are similar to the Eady model (cf. Figs. 5 and 2a). A localized disturbance near the tropopause at $t = -48$ h moves east and develops rapidly downstream during the cyclogenesis process around $t = 0$. The packet continues east during the next 48 h, exhibiting a structure similar to that of the linear solution: short-wavelength, shallow waves are located near the tropopause at the leading edge of the packet, with progressively longer-wavelength, deeper waves toward the packet peak. In contrast to the results of undamped linear theory, the observed packet exhibits a distinct upstream–downstream asymmetry, with an abrupt decline in packet amplitude just upstream from the peak. Because the trailing ray of the packet moves eastward, I conclude that, on average, these wave packets are convective instabilities; that is, upstream development is not observed.

A meridional cross section of PV through the developing packet exhibits nearly homogeneous values in the troposphere, with meridional gradients concentrated near the sloping tropopause (Fig. 6). This result is consistent with the idea that the appropriate theoretical model for

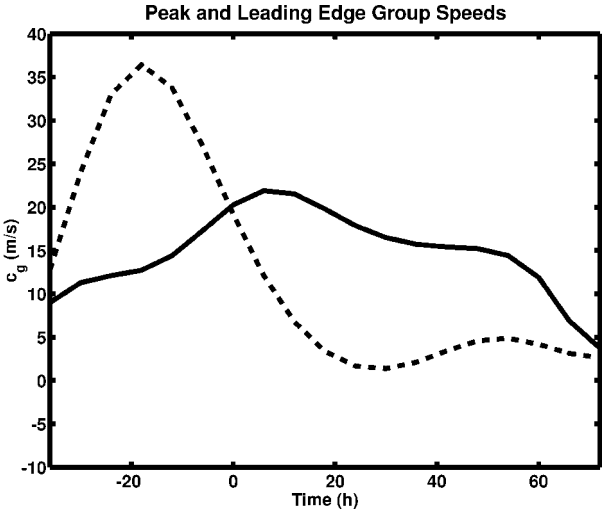

FIG. 10. Zonal group speed (m s^{-1}) as a function of lag (h) for the Pacific wave-packet peak (solid line) and leading edge (dashed line).

these events is based on homogeneous tropospheric PV. The classical Eady (1949) model provides the simplest example in this class. More realistic stability analyses show qualitatively similar results, with growing modes that peak near the surface and tropopause, maximum growth rates for wavelengths around 4000 km, and a short-wavelength cutoff (e.g., Hoskins and West 1979; Juckes 1998; Song and Nakamura 2000). Furthermore, Harnik and Lindzen (1998) showed that in the limit of vanishing PV gradients, mode solutions smoothly approach those for the classical Eady model.

b. Atlantic and 35°–40°N cyclones

Wave packets associated with cyclogenesis over the western North Atlantic Ocean (ATL) are qualitatively similar to the PAC events (Fig. 7). Prior to cyclogenesis, the packet appears to originate near the Gulf of Alaska and moves across North America. By $t = 0$, a well-developed packet extends across the North Atlantic Ocean, with the leading edge reaching western Europe by $t = 24$ h. The southern portion of the packet displays refraction into the subtropics at $t = 48$ h, similar to the PAC results.

The ensemble-mean evolution of all cyclones in the 35°–40°N belt is similar to the PAC and ATL cases (Fig. 8). Following a positive meridional wind anomaly located at the leading edge of the packet at $t = 0$, one finds that it amplifies and moves toward the packet peak with time. The PV field exhibits less in-phase structure with the meridional velocity field when compared to the PAC and ATL results, which may reflect less development in the NH sample. An asymmetry in packet amplitude near the peak at $t = 0$ gradually weakens toward a symmetric pattern as the packet travels downstream.

c. Wave-packet analysis

As described in section 3b, the structure of the wave packets is objectively analyzed to determine the packet peak and leading edge, as well as the packet zonal group speeds and wavelength as a function of position within the packet. At $t = 0$, the PAC packet leading edge exhibits a very good fit to an exponential profile with a coefficient of determination of $R^2 = 0.97$; there is an abrupt upstream edge to the packet just west of the packet peak (Fig. 9a). Wavelength within the packet increases from ≈3500 km at the peak to ≈4000 km 50° longitude to the east of the peak (Fig. 9b). At $t = 48$ h, the leading edge retains an exponential profile ($R^2 = 0.96$), with more wave activity upstream from the peak than at $t = 0$ (Fig. 9c). Wavelength within the packet decreases from ≈4000 km at the peak to ≈2800 km at the leading edge (Fig. 9d). Given observations of a climatological decrease in wavelength across the North Pacific (Chang and Yu 1999), it is possible that some of this decrease may be due to an along-stream decrease in the jet-level winds.

Figure 10 shows the zonal group speed of the PAC packet peak and leading edge as a function of time, with an error range of ≈5 m s^{-1}. Prior to $t = 0$, the leading edge accelerates to a peak speed of about 35 m s^{-1} and then decreases. At $t = 0$ the leading-edge group speed of 19 m s^{-1} compares with 24 m s^{-1} for the background flow. The packet peak group speed at $t = 0$ is 20 m s^{-1}, which compares with 36 m s^{-1} for the background flow. Note that the acceleration of the packet peak is evident at a later time than that of the leading edge. The acceleration of the leading edge and peak occur during the time when these features are located in strong winds of the Pacific jet.

Comparing the peak and leading-edge speeds, one expects the packet length to increase before $t = 0$ and then to decrease. An objective packet-length calculation confirms this expectation, with a length of 5700 km at $t = -36$ increasing to 8600 km at $t = 0$ and then decreasing to 5800 km at $t = 48$. This result suggests that wave packets may be focussed in the Pacific jet by an along-stream decrease in group speed. Such an effect has been predicted theoretically (Esler and Haynes 1999) and has not been found in previous observational studies (Chang and Yu 1999). This result may also be due to the compositing technique, with the expectation that packet length should decrease after $t = 0$ because of phase scrambling. However, given the plausible connection with the Pacific jet stream, it is suggested that future work should test the idea that strong along-jet variability can lead to packet focusing.

ATL and NH packet analyses at $t = 0$ confirm an exponential leading profile, with $R^2 = 0.96$ and $R^2 = 0.99$, respectively (Figs. 11a, 12a). These samples also exhibit increasing wavelength toward the leading edge at $t = 0$, which reverses by $t = 48$ h, such that the wavelength decreases approximately linearly from the

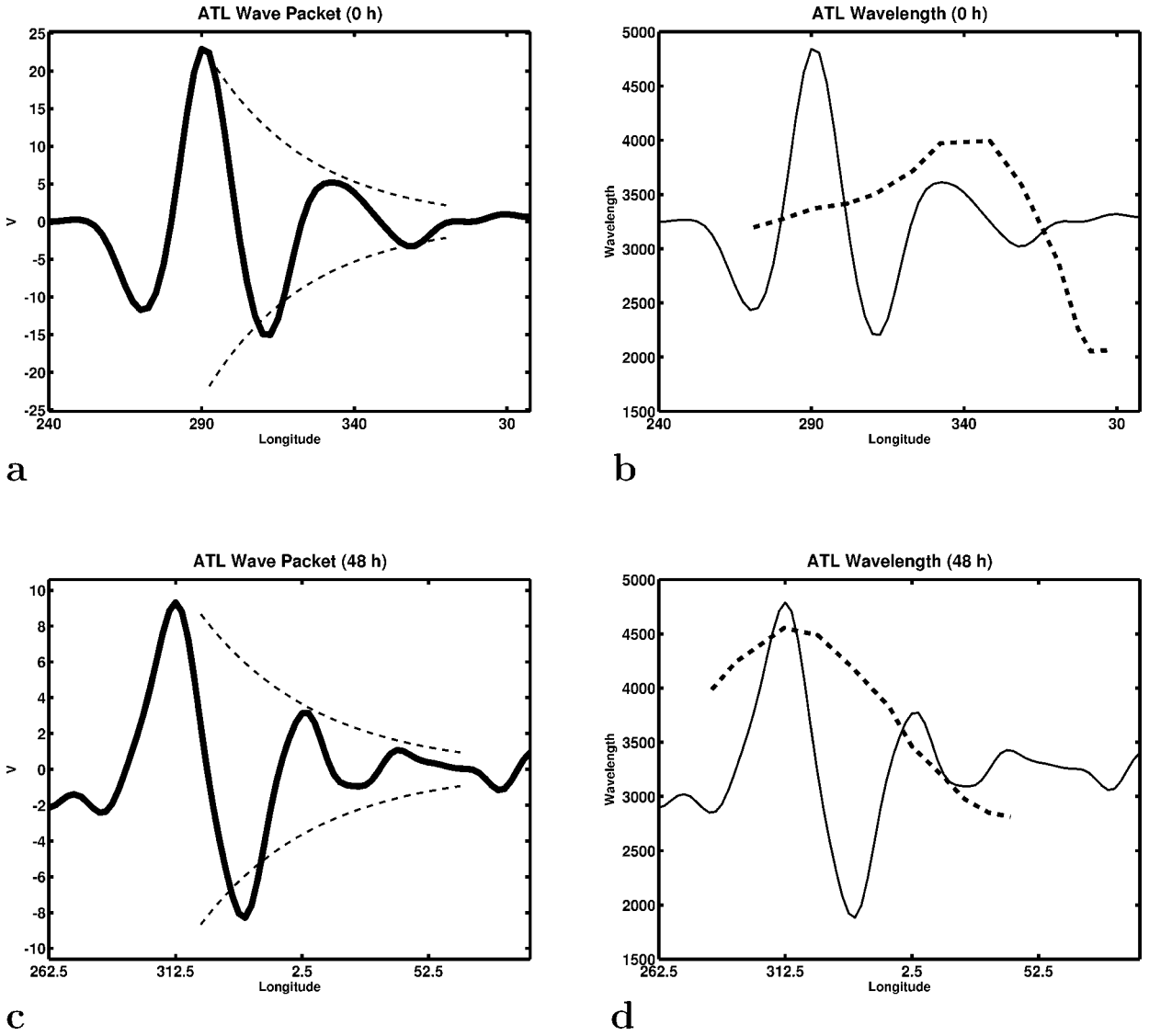

FIG. 11. As in Fig. 9, except for Atlantic wave packets. The packet analysis is taken along 42.5°N at $t = 0$ and 45°N at $t = 48$ h.

peak toward the leading edge (Figs. 11d, 12d). Wavelength at the leading edge at $t = 48$ h in all three samples (PAC, ATL, and NH) is ≈2500–3000 km, whereas the wavelength at the peak is ≈4000–5000 km.

Results of the packet analysis confirm several aspects of linear theory and suggest that impulsively produced packets rapidly assume the structure predicted for a spatiotemporal instability. These results also suggest that the wavelength of maximum growth rate is approximately 4000 km, and the ''short-wave cutoff'' for the storm tracks is approximately 2500 km. Where the results conflict with linear theory is mainly in the speed of the packet peak and leading edge. Previous idealized modeling studies have also found that the peak of mature packets moves at nearly the same speed as the leading edge because of nonlinear effects (Swanson and Pierrehumbert 1994). However, an additional complicating factor that affects the observed cases to an unknown extent relative to nonlinearity is the strong zonal variations of the background flow on the scale of the packet; this property may play an important role in focusing (and defocusing) PAC packets, as described earlier.

d. Dominant ray paths

In an effort to track packets for longer periods of time, I consider here subsamples of the full ensemble of cases that share common peak ray paths, which are defined as follows: At each analysis time (from $t = 0$ h to $t = 72$ h, every 24 h), the first local extremum downstream from the ensemble-mean packet packet peak is determined. This downstream location is then

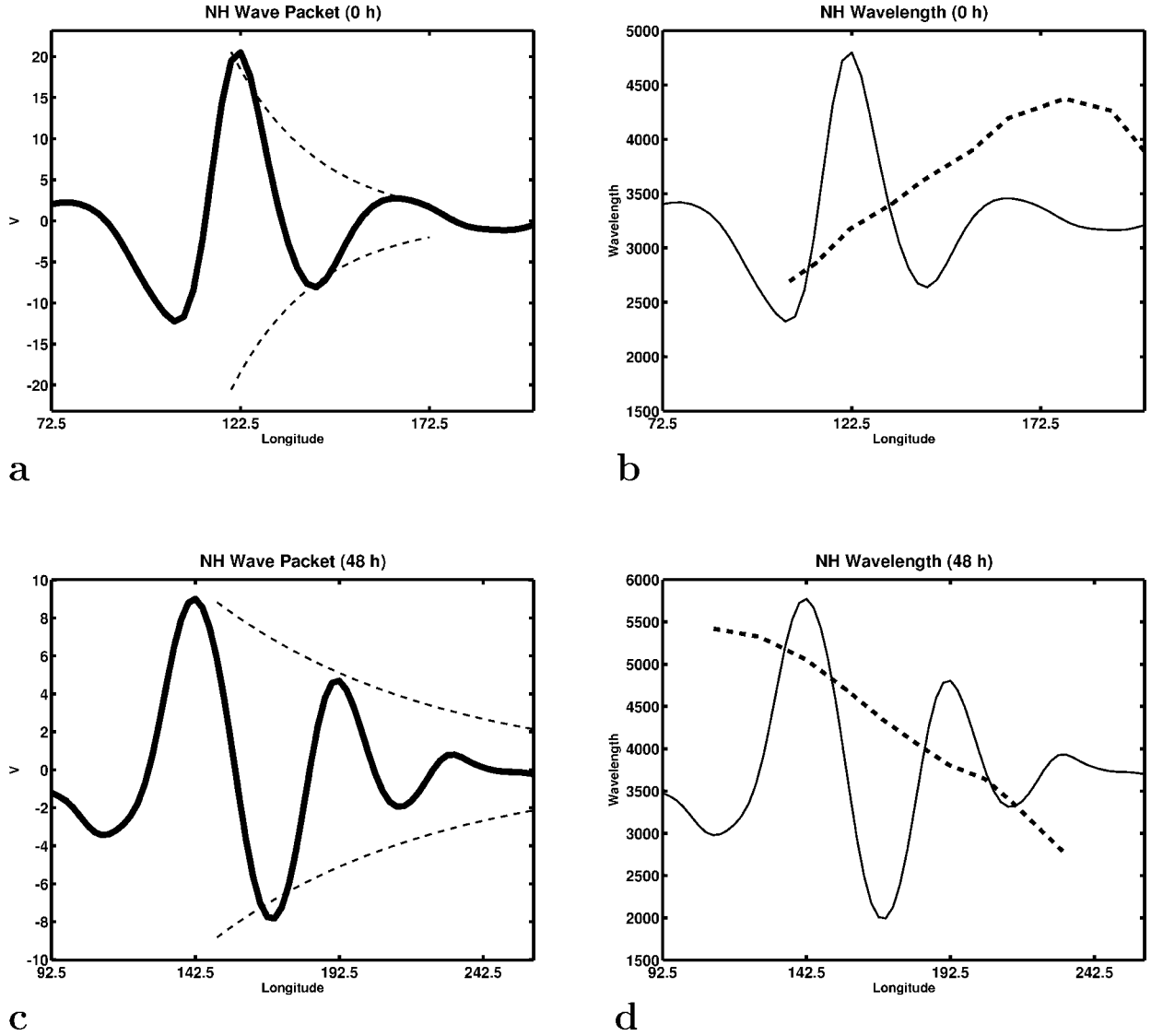

FIG. 12. As in Fig. 9, except for Northern Hemisphere wave packets. The packet analysis is taken along 40°N.

used to filter the sample to exclude cases that do not have a local extremum of the correct sign within ±10° latitude and longitude of the ensemble mean location. This process is repeated at the next analysis time using the filtered-sample ensemble mean. At 72 h, the PAC and ATL sample sizes are reduced to 83 and 107 events, respectively.

Figure 13 shows the dominant PAC and ATL peak rays relative to the November–March climatological 300-hPa wind speed for lags of −48 to 120 h. PAC packets originate north of the Himalaya Plateau, cross the Pacific, and then enter the Atlantic jet. ATL packets originate over western North America, cross the Atlantic, and then refract equatorward toward the subtropical jet that extends from North Africa to southern Asia. Based on the common ray paths over western North America, I conclude that Pacific wave packets often seed the Atlantic storm track; however Atlantic wave packets may not seed the Pacific storm track as effectively because the equatorward refraction of the ATL events places them south of the Himalaya Plateau, whereas PAC packets originate to the north of the plateau.

For the NH cases, a Hovmöller diagram of ensemble-mean 300-hPa meridional wind for a sample that is ray-filtered to 144 h (137 cases) shows a highly coherent signal that circumnavigates the hemisphere over 10 days (Fig. 14). The phase speed of individual eddies is ≈10 m s^{-1}, and the group speed of the packet peak is ≈35 m s^{-1}. These results are qualitatively similar to Chang (1993, his Fig. 3), although they are derived here for cases that originate from distinct cyclogenesis events as compared to a linear regression over all baroclinic waves and winter days.

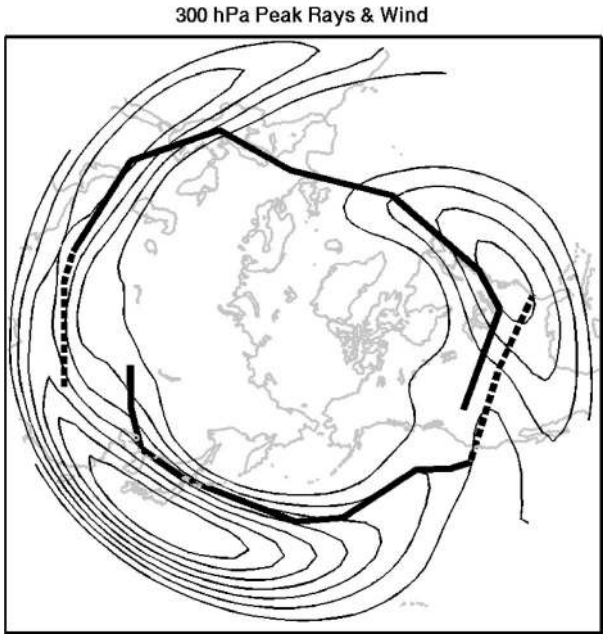

FIG. 13. Dominant rays for the Pacific and Atlantic wave packets. Heavy lines show the trajectory of the packet peak for the period $t = -48$ h to $t = 96$ h; dashed lines connect the peak to the leading edge at $t = 96$ h; and thin lines show the climatological magnitude of the 300-hPa wind for Nov–Mar 1949–99. Contours are drawn every 5 m s^{-1} starting with 20 m s^{-1}.

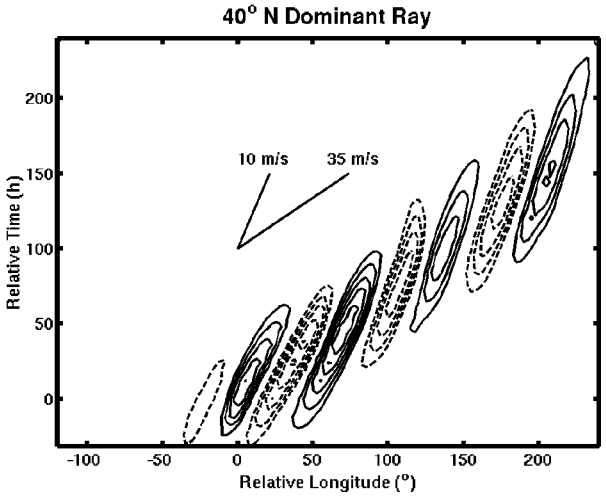

FIG. 14. Dominant peak ray for the Northern Hemisphere wave packets. The Northern Hemisphere wave-packet sample is filtered to a smaller subsample sharing a common ray path for the packet peak out to $t = 144$ h. Anomaly meridional wind is contoured every 2 m s^{-1}, with negative values dashed and the zero contour suppressed. Reference lines with slopes showing speeds of 10 and 35 m s^{-1} represent the approximate peak phase and group speed, respectively.

5. Conclusions

An observational analysis has been performed on a large sample of cyclogenesis events over the western North Pacific Ocean to document the developing wave packets that spread across the Pacific Ocean and to test theoretical predictions on packet structure and evolution. We find that the developing packet is preceded by an existing disturbance that reaches the western Pacific from the poleward side of the Himalaya Plateau. The leading edge of the packet crosses North America at tropopause level approximately 72 h after the initial disturbance reaches the Asian coastline.

Packet structure rapidly assumes the form of a spatiotemporal instability, with an exponential amplitude profile downstream from the leading edge. In contrast to undamped packets in linear theory, there is an abrupt edge to the observed wave packet just upstream from the packet peak. The vertical structure of the packet is similar to linear packets in the Eady (1949) model, with deep waves near the packet peak that become progressively shallower and concentrated near the tropopause as one moves toward the leading edge. Local wavelength within the packet at tropopause level increases from 3500 km at the peak to 4000 km downstream from the peak early in the life of the packet. One interpretation of this observation is that longer-wavelength unstable waves grow downstream from a smaller-scale precursor disturbance that approaches a region of enhanced surface baroclinicity. At later times, the local wavelength reaches a maximum of about 4000 km near the packet peak and decreases approximately linearly to about 2500 km near the leading edge. These values compare closely to expectations from linear theory based on the range of unstable wavelengths in the Eady (1949) model.

As predicted by theory, the group speed of the leading edge is bounded above by the background-flow speed, whereas the peak moves at about half the speed of the jet-level winds. Moreover, these speeds exhibit significant time dependence, such that the packet length changes with time; in particular, it decreases as the packet crosses the North Pacific Ocean. This along-stream decrease in group speed may help to focus the wave activity in the packet, although it is also possible that this asymmetry may be related to the compositing technique. A nonlinear version of this effect has been predicted theoretically (Esler and Haynes 1999), although the observations suggest a linear effect.

Similar results are found for cyclogenesis samples over the western North Atlantic and all longitudes at 35°–40°N. Furthermore, the Pacific and Atlantic results taken together suggest how effectively these storm tracks seed one another with precursor disturbances. It appears that Pacific wave packets may have a greater effect on the Atlantic storm track than Atlantic wave packets have on the Pacific storm tracks. This conclusion follows from Fig. 13, which shows that Atlantic wave packets refract equatorward onto the subtropical jet, passing south of the region that is the source for the Pacific wave-packet sample. Given the longer distance that Atlantic packets must travel to reach the Pacific storm track, we suspect that they may also suffer greater subtropical attenuation.

The results of this work suggest a need for better understanding of packet evolution in flows with large along-stream variation. Such variations in the Pacific and Atlantic jets often occur on scales similar to, or smaller than, the packet. For example, near the date line, the 300-hPa meridional PV gradient appears to have less zonal variation than the wind speed (cf. Figs. 3c and 13). These flow variations may affect local wave propagation so as to focus the packets in the western Pacific, as was suggested by the packet-length calculation. A second issue in along-stream variability concerns the jet-seeding problem. Since it appears that Pacific and Atlantic wave packets are unlikely to circumnavigate the hemisphere and reenter the poleward side of the Pacific jet, further work is needed to determine the origin of the Pacific wave-packet precursor disturbances originating poleward of the Himalaya Plateau.

Acknowledgments. This research was supported by the National Science Foundation through Grants ATM-9980744 and ATM-0228804. The comments of two anonymous reviewers helped clarify portions of the manuscript.

REFERENCES

Briggs, R. J., 1964: *Electron-Stream Interaction with Plasmas.* MIT Press, 187 pp.

Chang, E. K. M., 1993: Downstream development of baroclinic waves as inferred from regression analysis. *J. Atmos. Sci.,* **50,** 2038–2053.

——, 1999: Characteristics of wave packets in the upper troposphere. Part II: Seasonal and hemispheric variations. *J. Atmos. Sci.,* **56,** 1729–1747.

——, 2000: Wave packets and life cycles of troughs in the upper troposphere: Examples from the Southern Hemisphere summer season of 1984/85. *Mon. Wea. Rev.,* **128,** 25–50.

——, and I. Orlanski, 1993: On the dynamics of a storm track. *J. Atmos. Sci.,* **50,** 999–1015.

——, and D. B. Yu, 1999: Characteristics of wave packets in the upper troposphere. Part I: Northern Hemisphere winter. *J. Atmos. Sci.,* **56,** 1708–1728.

Cressman, G. P., 1948: On the forecasting of long waves in the upper westerlies. *J. Meteor.,* **5,** 44–57.

Eady, E. T., 1949: Long waves and cyclone waves. *Tellus,* **1** (3), 33–52.

Esler, J. G., and P. H. Haynes, 1999: Mechanisms for wave packet formation and maintenance in a quasigeostrophic two-layer model. *J. Atmos. Sci.,* **56,** 2457–2490.

Farrell, B. F., 1983: Pulse asymptotics of three-dimensional baroclinic waves. *J. Atmos. Sci.,* **40,** 2202–2209.

Gyakum, J. R., P. J. Roebber, and T. A. Bullock, 1992: The role of antecedent surface vorticity development as a conditioning process in explosive cyclone intensification. *Mon. Wea. Rev.,* **120,** 1465–1489.

Harnik, N., and R. S. Lindzen, 1998: The effect of basic-state potential vorticity gradients on the growth of baroclinic waves and the height of the tropopause. *J. Atmos. Sci.,* **55,** 344–360.

Hoskins, B. J., and N. V. West, 1979: Baroclinic waves and frontogenesis. Part II: Uniform potential vorticity jet flows—Cold and warm fronts. *J. Atmos. Sci.,* **36,** 1663–1680.

Huerre, P., and P. A. Monkewitz, 1990: Local and global instabilities in spatially developing flows. *Annu. Rev. Fluid Mech.,* **22,** 473–537.

Juckes, M., 1998: Baroclinic instability of semi-geostrophic fronts with uniform potential vorticity. I: An analytic solution. *Quart. J. Roy. Meteor. Soc.,* **124,** 2227–2258.

Lee, S., and I. M. Held, 1993: Baroclinic wave packets in models and observations. *J. Atmos. Sci.,* **50,** 1413–1428.

Lim, G. H., and J. M. Wallace, 1991: Structure and evolution of baroclinic waves as inferred from regression analysis. *J. Atmos. Sci.,* **48,** 1718–1732.

Namias, J., and P. F. Clapp, 1944: Studies of the motion and development of long waves in the westerlies. *J. Meteor.,* **1,** 57–77.

Orlanski, I., and J. J. Katzfey, 1991: The life cycle of a cyclone wave in the Southern Hemisphere. Part I: Eddy energy budget. *J. Atmos. Sci.,* **48,** 1972–1998.

——, and E. K. M. Chang, 1993: Ageostrophic geopotential fluxes in downstream and upstream development of baroclinic waves. *J. Atmos. Sci.,* **50,** 212–225.

——, and B. Gross, 2000: The life cycle of baroclinic eddies in a storm track environment. *J. Atmos. Sci.,* **57,** 3498–3513.

Pedlosky, J., 1987: *Geophysical Fluid Dynamics.* 2d ed. Springer-Verlag, 710 pp.

Pierrehumbert, R. T., 1984: Local and global baroclinic instability of zonally varying flow. *J. Atmos. Sci.,* **41,** 2141–2162.

——, and K. L. Swanson, 1995: Baroclinic instability. *Annu. Rev. Fluid Mech.,* **27,** 419–467.

Simmons, A. J., and B. J. Hoskins, 1979: The downstream and upstream development of unstable baroclinic waves. *J. Atmos. Sci.,* **36,** 1239–1254.

Song, Y., and N. Nakamura, 2000: Eady instability of isolated baroclinic jets with meridionally varying tropopause height. *J. Atmos. Sci.,* **57,** 46–65.

Swanson, K., and R. T. Pierrehumbert, 1994: Nonlinear wave packet evolution on a baroclinically unstable jet. *J. Atmos. Sci.,* **51,** 384–396.

Whitaker, J. S., and A. Barcilon, 1992: Type B cyclogenesis in a zonally varying flow. *J. Atmos. Sci.,* **49,** 1877–1892.